

# The Kormendy relation for early-type galaxies. Dependence on the magnitude range.

A. Nigoche-Netro<sup>1</sup>, A. Ruelas-Mayorga<sup>2</sup> and A. Franco-Balderas<sup>2</sup>

<sup>1</sup> Instituto de Astrofísica de Canarias (IAC), Vía Láctea s/n, 38200 La Laguna, Spain  
e-mail: alberto.n@imaff.cfmac.csic.es

<sup>2</sup> Instituto de Astronomía, Universidad Nacional Autónoma de México. Apartado Postal 70-264,  
México D.F., C.P. 04510  
e-mail: rarm@astroscu.unam.mx; alfred@astroscu.unam.mx

Preprint online version: February 23, 2019

## ABSTRACT

**Aims.** Due to a result from a recently published paper that states that the intrinsic dispersion of the Kormendy Relation (KR) for early-type galaxies (ETGs) depends on the magnitude range within which the galaxies are contained, we decided to investigate whether the magnitude range has also an influence over the values of the coefficients of the KR;  $\alpha$  (zero point) and  $\beta$  (slope). We perform numerical simulations and analysis of these coefficients for 4 samples of galaxies, which contain an approximate total of 9400 ETGs in a relatively ample magnitude range ( $\langle \Delta M \rangle \sim 6$  mag).

**Methods.** We calculate the values of the coefficients of the KR in two ways: i) We consider the faintest galaxies in each sample and we progressively increase the width of the magnitude interval by inclusion of the brighter galaxies (increasing magnitude intervals), and ii) we consider narrow magnitude intervals of the same width ( $\Delta M = 1.0$  mag) over the whole magnitude spectrum available (narrow magnitude intervals).

**Results.** The main results we find are as follows: i) In both increasing and narrow magnitude intervals the KR coefficients change systematically as we consider brighter galaxies, ii) non-parametric tests show that the fluctuations in the values of slope of the KR are not products of chance variations and that there is evidence of an underlying trend, and iii) this trend shows a maximum around absolute magnitude  $M_B \sim -18 \pm 1$ .

**Conclusions.** The analysis of the results makes us conclude that the values of the KR coefficients depend on the width of the magnitude range and the brightness of galaxies within the magnitude range. This dependence is due to the fact that the distribution of galaxies in the  $\log(r_e)$ - $\langle \mu \rangle_e$  plane depends on luminosity and that this distribution is not symmetrical, that is, the geometric shape of the distribution of galaxies in the  $\log(r_e)$ - $\langle \mu \rangle_e$  plane plays an important role in the determination of the values of the coefficients of the KR.

**Key words.** Galaxies: Elliptical and lenticular –Galaxies: Fundamental parameters

## 1. Introduction

It is a well known fact that the structural parameters of ordinary ETGs follow the Fundamental Plane (FP) relation (Djorgovsky & Davis 1987, Dressler *et al.* 1987). The FP relation is usually expressed as a correlation among the *logarithm of the effective radius* ( $\log(r_e)$ ), *effective mean surface brightness* ( $\langle \mu \rangle_e$ ) and *logarithm of the central velocity dispersion* ( $\log(\sigma_0)$ ), and is expressed mathematically with the following equation:

$$\log(r_e) = a \log(\sigma_0) + b \langle \mu \rangle_e + c \quad (1)$$

The FP relation is a direct consequence of the dynamical equilibrium condition (virial theorem) and of the regular behaviour of both the mass-luminosity ratio and of the galactic structure of the ETGs along all the luminosity range. Due to its small intrinsic dispersion ( $\sim 0.1 \text{ dex}$  in  $r_e$  and  $\sigma_0$  and  $\sim 0.1 \text{ mag}$  in  $\langle \mu \rangle_e$ ) the FP is considered a powerful tool in measuring galactic distances and also in studies of galactic formation and evolution (Kjærgaard *et al.* 1993, Jorgensen *et al.* 1996, Jorgensen *et al.* 1999, Kelson *et al.* 1997).

A physically significant projection of the FP is the correlation between  $\log(r_e)$  and  $\langle \mu \rangle_e$ , known as the Kormendy relation (KR):

$$\langle \mu \rangle_e = \alpha + \beta \log(r_e) \quad (2)$$

Several studies demonstrate that the ETGs in clusters define the KR with an intrinsic dispersion of approximately  $0.4 \text{ mag}$  in  $\langle \mu \rangle_e$  (Hamabe & Kormendy 1987, Hoessel *et al.* 1987, Sandage & Peremulter 1991, Sandage & Lubin 2001, La Barbera *et al.* 2003). Recent studies show that low-density-environment ETGs and isolated ETGs also follow the KR with the same coefficients and intrinsic dispersion as do ETGs in clusters (Reda *et al.* 2004, Nigoche-Netro *et al.* 2007). On the other hand, previous studies demonstrated that ETGs (plus bulges of spiral galaxies) formed two distinct families on the structural parameters plane; i.e. the family of bright ETGs ( $M_B \leq -18$ ) that follows the KR and the family of dwarf ETGs ( $M_B > -18$ ) with more disperse and heterogeneous properties (their effective parameters range over a wide interval for the same total luminosity) (Capaccioli *et al.* 1992). Subsequently Graham & Guzmán (2003) showed that the difference between the bright elliptical (bright E) and the dwarf elliptical (dE) galaxies is only apparent and that there is a continuous structural relation between both classes. They say that the different behaviour presented by the bright E and the dE galaxies in the  $\log(r_e) - \langle \mu \rangle_e$  plane and the variations in the value of the slope of the relation do not imply a different formation mechanism, rather it may be interpreted as a systematic change in the shape of the light-profile with galactic magnitude ( $M$ ). This result, together with the fact that the intrinsic dispersion of the KR depends on the magnitude range (Nigoche-Netro *et al.* 2007, Nigoche-Netro 2007) prompted us to study the behaviour of the coefficients of the KR as functions of the magnitude range. If indeed, the values of the coefficients of the KR depend on the magnitude range within which the galaxies are contained, and this fact is not considered when performing comparisons of galaxy samples such as the dependence of the KR on the environment, on redshift or on wavelength, the differences which might be found may be misinterpreted.

In this paper, we present a compilation of 4 samples of ETGs which in total contain approximately 9400 galaxies and cover a relatively ample magnitude range ( $\Delta M \sim 6 \text{ mag}$ ). Using these data we analyze the behaviour of the coefficients of the KR with respect to several characteristics of the magnitude range. We also present numerical simulations of the distribution of the galaxies on the  $\log(r_e) - \langle \mu \rangle_e$  plane. These simulations allow us to reproduce in a reasonable manner the results we obtain from the real samples of galaxies.

This paper is organized as follows. In section 2, we present the different samples used in the analysis of the KR. Section 3 describes the fitting method used in calculating the KR coefficients, as well as the behaviour of the  $\beta$  coefficient with respect to the absolute magnitude range. Section 4 presents numerical simulations of the distribution of the galaxies on the  $\log(r_e) - \langle \mu \rangle_e$  plane and finally in section 5 the conclusions are presented.

## 2. The samples

We use a Sloan Digital Sky Survey (SDSS) sample of 8666 ETGs (Bernardi *et al.* 2003) in filters  $g^*$ ,  $r^*$ ,  $i^*$  and  $z^*$  (total absolute magnitude range  $-18 \geq M_{g^*} > -24.1$  and its equivalent in other filters) as well as a sample of 626 ETGs in the Johnson V filter ( $-16 \geq M_V > -22$ ) from 7 Abell clusters (WINGS project, Fasano *et al.* 2002, Varela 2004), a sample in filter Gunn r ( $-17 \geq M_{Gr} > -24$ ) with 196 ETGs from the Coma cluster (Milvang-Jensen 1997, Aguerri *et al.* 2005) and a 54 ETGs sample in the filter Gunn r ( $-18 \geq M_{Gr} > -22$ ) from the Hydra cluster (Milvang-Jensen 1997).

All the samples are redshift-homogeneous (the galaxies are contained within a narrow redshift interval), except for the SDSS sample which cover a relatively ample redshift interval ( $0.01 \leq z \leq 0.3$ ). This sample is magnitude-limited (Bernardi *et al.* 2003b). Besides, within large volumes there could be evolution effects of the parameters of the galaxies. So, in order to have a representative sample of the universe in a given volume without any evolution effects it is important to consider narrow redshift intervals. Bernardi *et al.* 2003b recommend  $\Delta z = 0.04$ . This value comes from the sizes of the largest structures in the universe seen in numerical simulations of the cold dark matter family of models (Colberg *et al.* 2000). It is also well known that the SDSS photometry underestimates the luminosity of the brightest objects in crowded fields (Bernardi *et al.* 2007, Bernardi *et al.* 2007b).

To probe the possible evolution effects and the photometric bias of the brightest galaxies, we have built a subsample from the SDSS in the redshift interval  $0.04 \leq z \leq 0.08$ . This subsample has 1670 galaxies in each filter and cover a magnitude range  $\Delta M \sim 4 \text{ mag}$  ( $-18.5 \geq M_{g^*} > -22.9$  and its equivalent in other filters). This subsample will be referred to, from now on, as homogeneous sample from the SDSS.

In Table 1 we present relevant information (number of galaxies, magnitude range and redshift) for the samples of galaxies we use in this paper. The magnitude range information is given in relation to the different filters used (from the literature) and also the approximate range for the B-magnitude (calculated by us). The transformation to the B filter was accomplished by use of the following equations:  $B - \text{Gunn } r = 1.15$  (Milvang-Jensen 1997) and  $B - V = 0.92$  (Michard 2000). The filters  $g^*$ ,  $r^*$ ,  $i^*$  and  $z^*$  correspond approximately to the Johnson-Morgan-Cousins filters B, V,  $R_c$  and  $I_c$  respectively (Fukugita *et al.* 1996).

**Table 1.** Name, Number of galaxies, Magnitude range (according to the papers where the samples were taken from), Approximate magnitude range in the B-Filter (calculated by us) and redshift of the different galaxy samples compiled in this work. In the 7 Abell cluster sample we include the following clusters: A147, A168, A193, A2457, A2589, A2593, and A2626.

Sample	N	Magnitude range	Approximate magnitude range in the B-filter	$z$
7 Abell clusters (V filter)	626	$-16.0 \geq M_V > -22.0$	$-15.1 \geq M_B > -21.1$	0.048
Coma cluster (Gunn r filter)	196	$-17.0 \geq M_{Gr} > -24.0$	$-15.9 \geq M_B > -22.9$	0.024
Hydra cluster (Gunn r filter)	54	$-18.0 \geq M_{Gr} > -22.0$	$-16.9 \geq M_B > -20.9$	0.014
SDSS (g* filter)	8666	$-18.0 \geq M_{g*} > -24.1$	$-18.0 \geq M_B > -24.1$	$\leq 0.3$
SDSS (r* filter)	8666	$-18.6 \geq M_{r*} > -24.7$	$-18.0 \geq M_B > -24.1$	$\leq 0.3$
SDSS (i* filter)	8666	$-19.0 \geq M_{i*} > -25.1$	$-18.0 \geq M_B > -24.1$	$\leq 0.3$
SDSS (z* filter)	8666	$-19.3 \geq M_{z*} > -25.3$	$-18.0 \geq M_B > -24.1$	$\leq 0.3$

All the samples consider the photometric parameters  $\log(r_e)$  and  $\langle \mu \rangle_e$  corrected for different biases (galactic extinction, K correction and cosmological dimming). These parameters as well as their uncertainties were taken directly from the different papers cited above, except for the parameters for the Abell samples which constitute a private communication from the WINGS project team (Fasano *et al.* 2002, Varela 2004), and those for Coma (data from Aguerri *et al.* 2005). In this last case, given that Aguerri *et al.* (2005) give information for effective surface brightness ( $\mu_e$ ) instead of effective mean surface brightness ( $\langle \mu \rangle_e$ ), we transform these data by using the following expression:

$$\langle \mu \rangle_e = \mu_e - F(n) \quad (3)$$

Where  $F(n)$  is a function of the Sérsic  $n$ -index (Graham & Driver 2005).

It is important to note that, according to the papers where the samples were taken from, the photometric parameters of the faint and bright ETGs in the Abell sample as well as the faint ETGs in the Coma sample were obtained using Sérsic profile-fits. Whereas for the bright ETGs from the other samples (which for the SDSS sample consists of the entire sample), these parameters were obtained using de Vaucouleurs  $r^{1/4}$  profile-fits.

According to Prugniel & Siemen (1997), the de Vaucouleurs profile-fits represent a good approximation to the Sérsic profile-fits for bright galaxies. In section 3.3 it will be shown that this approximation does not produce important biases to the results obtained in this paper.

Finally, an important characteristic of S0 galaxies is that, in general, the structural properties of their bulges show approximately the same homogeneity as those of E galaxies. Due to this fact, and because KR uses effective parameters, we use the photometric parameters from the whole galaxy in the case of bright Es, and from the bulge in the case of bright S0s. For dwarf galaxies we follow the same procedure: information from the whole galaxy for the dEs and from the bulge for the dS0s.

### 3. Kormendy relation

#### 3.1. Calculation of the Kormendy relation

The estimation of the KR coefficients may be severely affected by the fitting method and by the choice of dependent variable. The biases may be larger if there are measurement errors in the vari-

ables, if these errors are correlated and/or if there is intrinsic dispersion. The *Bivariate Correlated Errors and Intrinsic Scatter bisector* ( $BCES_{Bis}$ ) fit (Isobe *et al.* 1990, Akritas & Bershadsky 1996) is a statistical model that takes into account the different sources of bias mentioned above, which are precisely those that affect our samples. In this work we use the  $BCES_{Bis}$  method for the determination of the KR coefficients.

From the photometric parameters of the different galaxy samples, we calculate the coefficients of the KR in different magnitude ranges, the uncertainties of the coefficients, the correlation coefficient (Pearson Statistics) and the intrinsic dispersion of the KR (subtracting in quadrature from the intrinsic dispersion in  $\langle \mu \rangle_e$  the residues dispersion due to the measurement errors of  $\langle \mu \rangle_e$  and  $\log(r_e)$ ) (La Barbera *et al.* 2003). According to La Barbera *et al.* (2003), for the calculation of the intrinsic dispersion it is necessary to have the measurement errors in  $\langle \mu \rangle_e$  and  $\log(r_e)$ , these errors come directly from the papers from which we take the galaxy samples (see section 2), while the errors in the KR coefficients were calculated by us following Akritas & Bershadsky (1996) in  $1\sigma$  intervals.

The KR coefficients were calculated both in increasing magnitude intervals, as well as in narrow magnitude intervals. This allows us, among other things, to characterize the behavior of the KR coefficients with respect to the width of the magnitude range and the brightness of galaxies within the magnitude range so the results obtained may be utilized as reference for other studies in which different magnitude ranges are used. In Tables A.1 and A.2 (Appendix A) we present the results for the values of the coefficients of the KR for the different samples of galaxies and for different magnitude intervals.

### 3.2. Behaviour of the Kormendy relation coefficients with respect to absolute magnitude range

From the analysis of the data for our different samples we notice that the intrinsic dispersion of the KR ( $\sigma_{KR}$ ), as clearly stated by Nigoche-Netro *et al.* (2007), changes appreciably each time we include brighter galaxies in the samples (upper magnitude cut-off), that is to say when we use increasing magnitude intervals (see Table A.1). We also notice that the correlation coefficient (R) for each fit diminishes considerably. Apart from these changes, we can also see changes in the coefficients of the KR and that these changes are larger than the associated errors for most of the cases (differences in the  $\beta$  coefficient may be as large as 65%). The distribution of the  $\beta$  coefficient may be seen on Fig. 1, where it is interesting to note that this distribution presents a maximum at  $M_B \sim -18 \pm 1$ . On the other hand, if we perform the KR analysis considering first the brightest galaxies in each sample and we include progressively the fainter galaxies (lower magnitude cut-off), the behaviour of the KR parameters is similar to that described above: both the intrinsic dispersion and the KR coefficient-values change systematically as we increase the width of the magnitude interval.

We also perform the analysis of the data using magnitude intervals that are narrow (see Table A.2), that is, considering galaxy samples in magnitude intervals of the same width and progressively brighter. For this case we can also see changes in the coefficients of the KR, however, the changes are less pronounced but still larger than the associated errors for most of the cases (differences in the  $\beta$  coefficients may be as large as 48%). We also find that the intrinsic dispersion of the KR is relatively low in all cases, and that the correlation coefficient is, on the average superior to

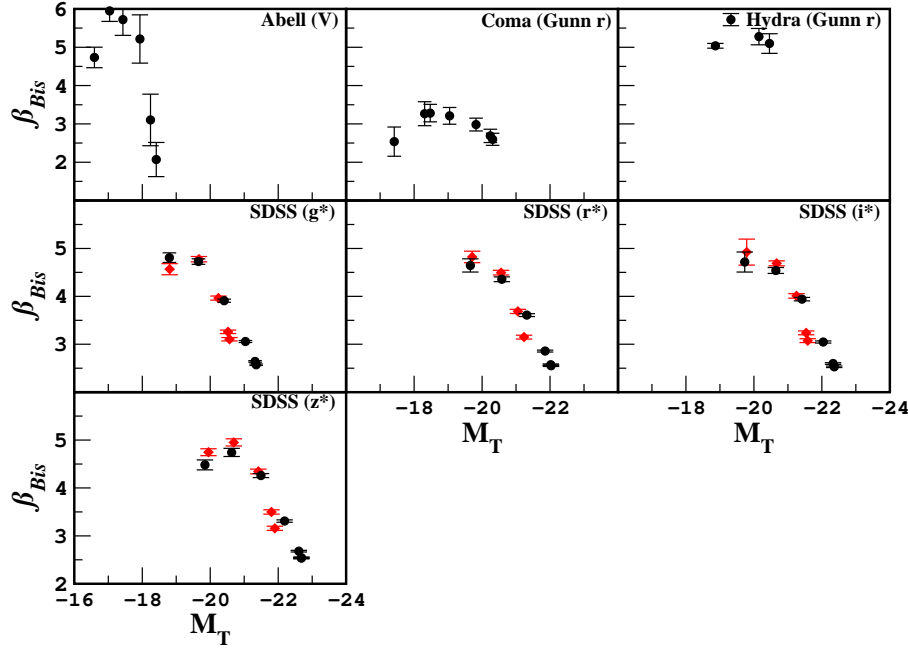


**Fig. 1.** Graph of the variation of the KR slope ( $\beta$ ) for the different samples of galaxies in increasing magnitude intervals (upper magnitude cut-off). This graphs shows the  $\beta$  coefficient obtained using the  $BCES_{Bis}$  method. Each point corresponds to the mean value of the total absolute magnitude of the galaxies contained in each magnitude interval (see table A.1). Filters  $g^*$ ,  $r^*$ ,  $i^*$  and  $z^*$  correspond approximately to Johnson-Morgan-Cousins filters B, V,  $R_c$  and  $I_c$  respectively (Fukugita et al. 1996). Diamonds represent the SDSS homogeneous sample.

0.9. The variation of the  $\beta$  coefficient when we consider narrow magnitude intervals may be seen on Fig. 2 where a dependence between the  $\beta$  coefficient and absolute magnitude appears to be hinted at. However, it may be possible for the  $\beta$  coefficient to be constant ( $\beta = 5$ ) and that the differences we find are the result of statistical fluctuations.

The question that  $\beta$  be constant and equal to 5 comes from the definition of absolute magnitude in terms of effective radius and effective mean surface brightness, that is:

$$M = \langle \mu \rangle_e - 5 \log(R_e) - 2.5 \log(2\pi) - 5 \log(D) + 5 \quad (4)$$

where  $R_e$  [arcsec] and  $D$  [pc] represent the effective radius and the distance to the object in question respectively and  $\langle \mu \rangle_e$  [mag/arcsec<sup>2</sup>] is the effective mean surface brightness.

If we consider the effective radius in kiloparsecs ( $r_e$ ) and a constant magnitude, we obtain the KR as follows:

$$\langle \mu \rangle_e = \alpha + 5 \log(r_e) \quad (5)$$

Which implies that

$$\beta = 5 \quad (6)$$

However, the observational data for  $\beta$  seem to move away from the expected value. In order to clear this point, it is necessary to apply non-parametric tests to make certain that the fluctuations in the values of the slope are not products of chance variations.

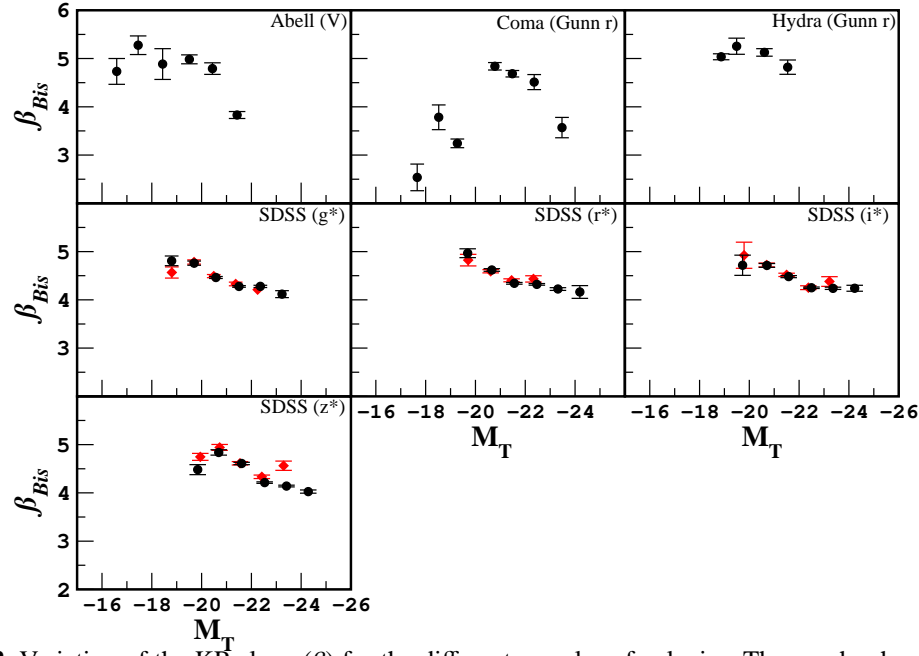


**Fig. 2.** Variation of the KR slope ( $\beta$ ) for the different samples of galaxies. The graphs show the  $\beta$  coefficient values obtained with the  $BCES_{Bis}$  method. Each point represent a 1 *mag* interval (mean value of the total absolute magnitude of the galaxies contained in each magnitude interval analyzed, see table A.2). Diamonds represent the SDSS homogeneous sample.

### 3.3. Hypothesis Tests for the evaluation of $\beta$ data

There are several non-parametric methods for the evaluation of sets of data (Bendat & Piersol 1966). One of the most popular is the chi-square test. This test measures the discrepancy between an observed probability density and a theoretical probability density (i.e. a normal distribution). Another important test, which does not *a priori* assume a specific distribution, is that known as run test. There is one particularly interesting non-parametric test (mean value test), which helps in finding out whether the data in question are distributed at random around a given value or whether this distribution is not a random one.

In Table 2 we show the results of the application of the tests to the different galaxy samples in increasing and narrow magnitude intervals. The null hypothesis of the mean value test (test 1) is that  $\beta$  has a normal distribution and that its mean value is 5 (we consider the data to have a measurement error equal to 10%), the null hypothesis of the run test (test 2) is that there is not an underlying trend in the  $\beta$  data and finally the null hypothesis of the chi-square test (test 3) is that the  $\beta$  data are random and that they follow a normal distribution. The percentages given in Table 4 refer to the confidence level with which we can reject the null hypothesis.

From Table 2 we can see that, on average, the null hypothesis may be rejected with a level of confidence of 95 %. This implies that there are strong reasons to believe that the mean value of  $\beta$  is not 5, that there is an underlying trend in the values of  $\beta$  and that the distribution of these values is not normal.

From the previous results there is a question that arise: Why is there an underlying trend in the values of  $\beta$  when we consider increasing and narrow magnitude intervals? A possible answer to this question is that the change in the value of the slope might be due to the fact that the distribution of the galaxies on the  $\log(r_e) - < \mu >_e$  plane depends on the luminosity (Fig. 3, see further

**Table 2.** Hypothesis Test for the evaluation of the  $\beta_{Bis}$  data from the different samples of galaxies. Tests 1, 2 and 3 correspond to the mean value, run and chi-square tests respectively. The null hypothesis of test 1 is that  $\beta$  has a normal distribution and that its mean value is 5 (we consider the data to have a measurement error equal to 10%), the null hypothesis of test 2 is that there is not an underlying trend in the  $\beta$  data and the null hypothesis of test 3 is that the  $\beta$  data are random and that they follow a normal distribution. The percentages refer to the level of confidence with which we can reject the null hypothesis.

	Test 1	Test 2	Test 3
<hr/> Sample (increasing magnitude intervals)			
Abell	94 %	81 %	...
Coma	99 %	89 %	...
Abell+Coma+Hydra	99 %	...	95 %
SDSS in each filter	99 %	96 %	...
SDSS sum of 4 filters	99 %	96 %	90 %
Abell+Coma+Hydra+SDSS sum of 4 filters	99 %	96 %	95 %
<hr/> Sample (1 <i>mag</i> interval)			
Abell	84 %	81 %	...
Coma	99 %	89 %	...
Abell+Coma+Hydra	99 %	...	95 %
SDSS in each filter	99 %	96 %	...
SDSS sum of 4 filters	99 %	96 %	90 %
Abell+Coma+Hydra+SDSS sum of 4 filters	99 %	96 %	95 %

details in Varela 2004, D’Onofrio *et al.* 2006, Nigoche-Netro *et al.* 2007). It could also be due to the geometrical shape of the galaxy distribution on this plane. If the distribution of galaxies takes a rectangular shape, fitting a straight line to these data will produce different results from a straight-line fit to a galaxy distribution that takes a triangular shape or any other shape. In the following section we present numerical simulations of the galaxy distribution on the  $\log(r_e) - \langle \mu \rangle_e$  plane that elucidate clearly the effects that the shape of the distribution of galaxies on this plane has over the values of the coefficients of the KR.

Here, it is important to note that the behaviour of the parameters of the KR in the bright regime is similar for all the samples, in other words, the use of the de Vaucouleurs profiles as an approximation of the Sérsic profiles (for bright galaxies in some samples) does not affect appreciably the behaviour of the parameters of the KR (Fig. 2). On the other hand, when we compare the behaviour of the  $\beta$  coefficient for the heterogeneous SDSS sample and the homogeneous SDSS sample (Figs. 1 and 2) we note that this behaviour is similar for both samples except for the brightest part, how-



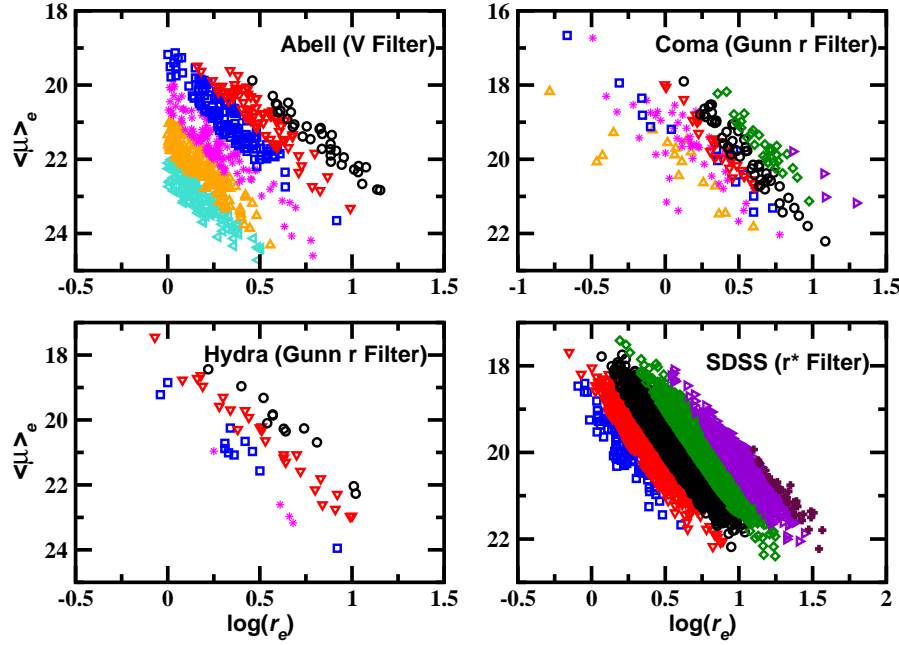


**Fig. 3.** Distribution of the Abell, Coma, Hydra and SDSS ( $r^*$  filter) galaxies on the  $\log(r_e) - \langle \mu \rangle_e$  plane. Each symbol represents a 1 mag interval. The circles represents the  $(-21, -22]$  mag interval.

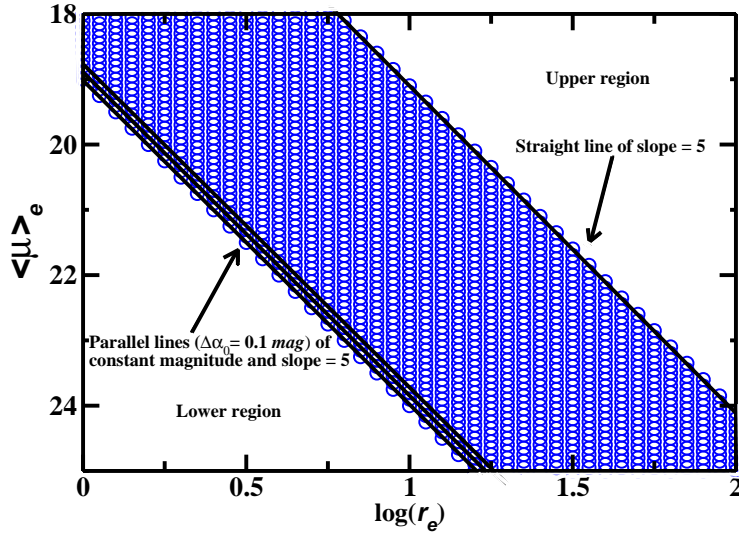


**Fig. 4.** Distribution of simulated galaxies on the  $\log(r_e) - \langle \mu \rangle_e$  plane. The data distribution consists in parallel lines of slope 5 which shift to brighter magnitude.

ever, it is precisely for these galaxies for which the photometry bias could be more pronounced. So it is not possible to say that the differences found are produced by evolution effects.

#### 4. Numerical simulations

To investigate whether the magnitude dependence of the KR coefficients is due to the geometric shape of the distribution of galaxies on the  $\log(r_e) - \langle \mu \rangle_e$  plane (geometrical effect), we perform numerical simulations for each one of our samples of galaxies (Fig. 4). The simulations consist in giving values to  $\log(r_e)$  in a similar radii range as that of the sample in question, fixing the

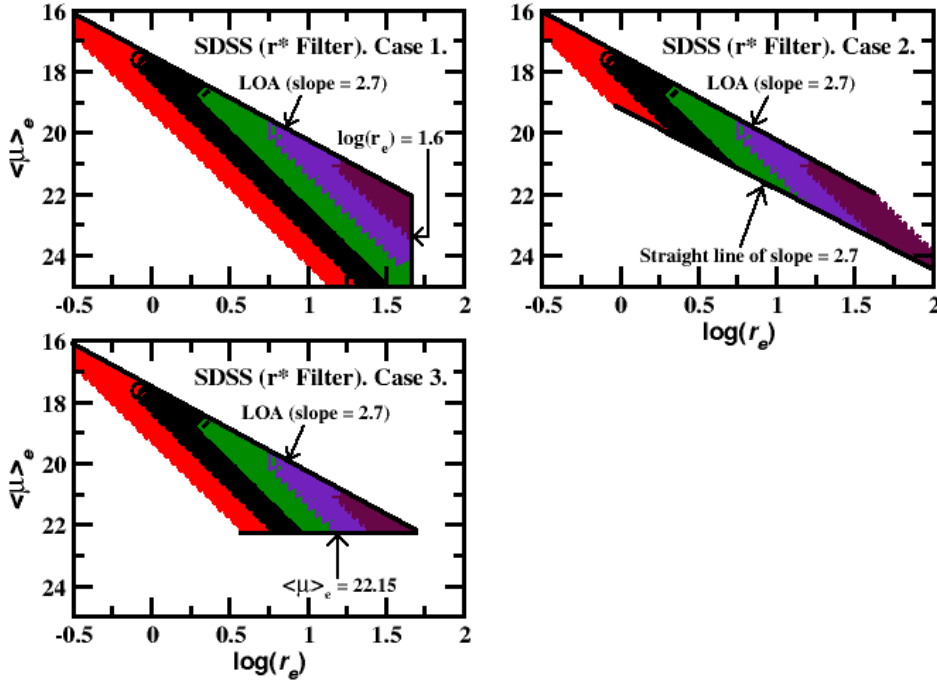


**Fig. 5.** Distribution of simulated SDSS galaxies ( $r^*$  filter) on the  $\log(r_e)$ -  $\langle \mu \rangle_e$  plane. Each symbol represents a 1 mag interval. The circles represents the  $(-21, -22]$  mag interval. Case 1: upper region of the diagram, limited by a straight line of slope 2.7 (LOA) (D’Onofrio et al. 2006) and radius limit ( $\log(r_e) \leq 1.6$ ) for all the magnitude intervals. Case 2: upper and lower regions of the diagram limited by a straight line of slope 2.7. Case 3: upper region of the diagram limited by a straight line of slope 2.7 and brightness limit ( $\langle \mu \rangle_e \leq 22.15$  mag/arcsec<sup>2</sup>) for all the magnitude intervals.

faintest zero-point ( $\alpha_0$ ) of this sample (it is equivalent to fixing a magnitude) and fixing a slope of 5 (expected slope considering the definition of total absolute magnitude). Then, we take the same range of  $\log(r_e)$ , a  $\alpha_0$  slightly brighter (we take increments of 0.1 mag) and the same slope of 5, and so on until we cover the whole range of brightness of the sample in question. The resulting data distribution consists in parallel lines of slope 5 which shift to brighter magnitude. Once the data are generated, we simulate the observed depopulation effect on the upper region of the galaxy distribution (Fig. 5). This depopulation is known as the exclusion zone (Bender *et al.* 1992) and may be characterized by a straight line (Line of Avoidance or LOA) that has a slope approximately equal to 2.7 (D’Onofrio *et al.* 2006). Since we do not know the way in which galaxies locations in the lower part of the  $\log(r_e)$  -  $\langle \mu \rangle_e$  plane behave, we consider the following 3 cases in the simulation of this region:

Case 1. It consists in setting a fixed limit-radius for all the magnitude intervals, so that the galaxies are contained within a triangle, one of whose sides is parallel to the  $\langle \mu \rangle_e$  axis.

Case 2. In this case we consider that the lower region of the diagram is limited by a 2.7-slope straight line, that is, there is an identical exclusion zone in this part of the diagram, as that observed in the upper part. Therefore the galaxies appear to be contained within a parallelogram and their distribution appears to be symmetric with respect to an axis that contains the barycenter of the galaxy distribution and is parallel to the  $\log(r_e)$  axis, we shall call this axis from now on the

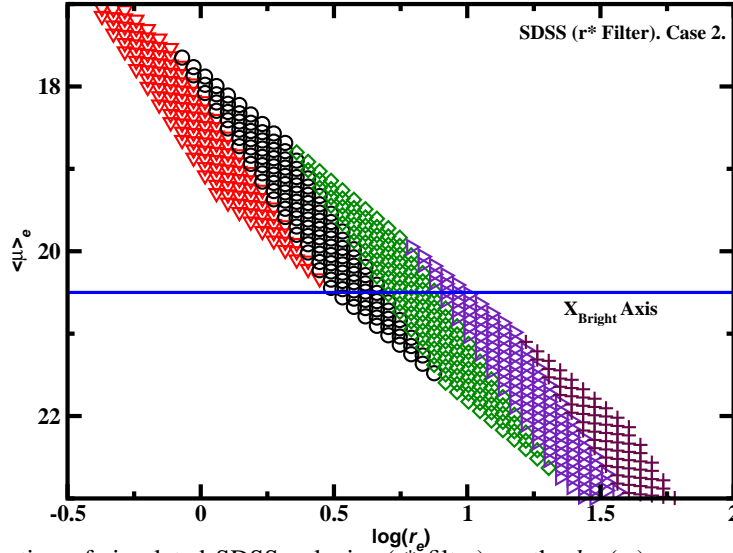


**Fig. 6.** Distribution of simulated SDSS galaxies ( $r^*$  filter) on the  $\log(r_e)$ -  $\langle \mu \rangle_e$  plane (Case 2). Each symbol represents a 1 mag interval. The solid line ( $X_{Bright}$ -axis) is a line of slope=0 that contains the barycenter of the distribution of the galaxies. The galaxy distribution is symmetrical under a reflection with respect to the  $X_{Bright}$ -axis and a  $180^\circ$  rotation with respect to a perpendicular line to the  $X_{Bright}$ -axis that contains the barycenter of the galaxy distribution.

$X_{Bright}$ -axis. Further details on the definition of the  $X_{Bright}$ -axis, as well as on the symmetry type discussed here, are given in Fig. 6.

Case 3. We consider the lower region as limited in brightness, so galaxies are contained within a triangle with one of its sides parallel to the  $\log(r_e)$  axis.

The results of the analysis of the KR show that when we consider increasing magnitude intervals (Table A.3), there are slope changes in all the cases, and these changes are always larger than the errors. We also find that the geometric shape of the distribution of galaxies changes each time we include brighter galaxies in the samples (Fig. 5). On the other hand, when we consider narrow 1-magnitude intervals (Table A.4), there are also slope changes (except for case 2), however, the changes are less pronounced but still larger than the errors and if the magnitude intervals are progressively narrower, then the changes diminish considerably getting ever closer to the value of 5, just as it occurs for the real samples. Finally, if the magnitude interval is equal to 0.1 mag then the slope is exactly equal to 5 since that is the way we define the samples.

It is important to mention that when we consider narrow magnitude intervals we are able to reproduce, in a reasonable manner, the  $\beta$  coefficient variations and the underlying trend (maximum at  $M_B \sim -18 \pm 1$ ) found for the real samples (except for case 2) (Fig. 7). We also find that the geometric shape of the distribution of galaxies changes systematically when we consider brighter magnitude intervals (except for case 2) (Fig. 5). We must remind the reader that Case 2 corresponds to a symmetrical galaxy distribution over the  $\log(r_e)$  -  $\langle \mu \rangle_e$  plane.

Moreover, we find that both the zero point ( $\alpha$ ) and the intrinsic dispersion ( $\sigma_{KR}$ ) of KR change systematically when we consider brighter galaxies. This latter result confirms the dependence of the intrinsic dispersion with the magnitude range as reported in Nigoche-Netro et al. 2007.

From the aforementioned, we may infer that the KR coefficients and its intrinsic dispersion depend on the width and brightness of the magnitude range. This dependence is caused by a ge-

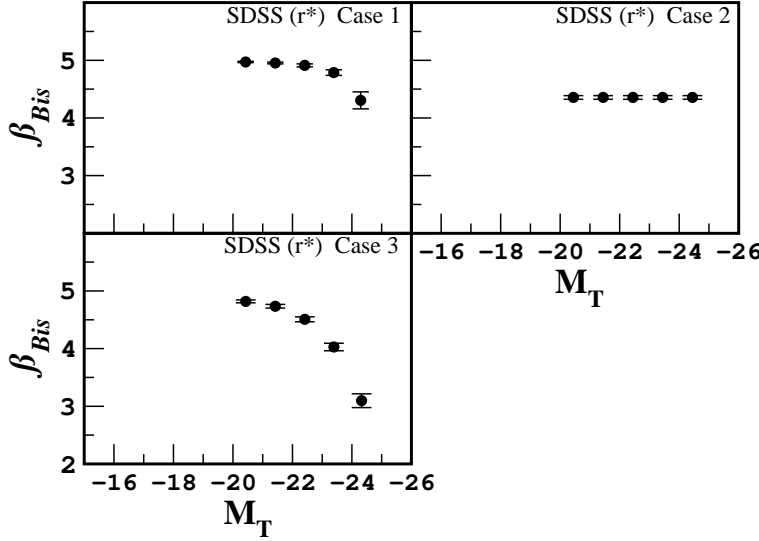


**Fig. 7.** Variation of the KR slope ( $\beta$ ) for one of the SDSS simulations ( $r^*$  filter). Graphs show the data for the  $\beta$  coefficient obtained by the  $BCES_{Bis}$  method. Each point represents a 1 mag interval (mean value of the total absolute magnitude of the galaxies contained in each magnitude range analyzed, see table A.4).

ometrical effect due to the fact that the distribution of the galaxies on the  $\log(r_e) - \langle \mu \rangle_e$  plane depends on luminosity and also to the fact that this distribution is not symmetrical with respect to the  $X_{bright}$ -axis, in other words, the geometric shape of the distribution of galaxies on the  $\log(r_e) - \langle \mu \rangle_e$  plane changes systematically as we consider brighter galaxies, and so the values of the KR coefficients change too, because the fitting of a straight line to a set of data does not give the same result for slope and intercept values for data distributed with a rectangular shape as for data distributed with a triangular shape or, for that matter, with another geometrical shape. In this sense, any other systematic restrictions imposed on a sample of galaxies, such as brightness cuts or effective radius cuts, will cause changes in the geometric shape of the distribution of galaxies. The more pronounced these changes are made, the more pronounced will be the changes in the values of the KR coefficients.

## 5. Conclusions

We have compiled 4 samples of ETGs with information for their photometric parameters  $\log(r_e)$  and  $\langle \mu \rangle_e$ , these samples contain a total of  $\sim 9400$  galaxies in a relatively ample magnitude range ( $\langle \Delta M \rangle \sim 6$  mag). From the values of their photometric parameters, we have made an analysis of the behaviour of the coefficients and intrinsic dispersion of the KR with respect to several characteristics of the magnitude range within which the galaxies are contained. The results from this study are presented as follows:

- We find that when we include in the samples galaxies which get progressively brighter (increasing magnitude intervals) or if we consider galaxy samples in progressively brighter fixed-width magnitude intervals (narrow magnitude intervals), the KR coefficients change and these changes result to be larger than the associated errors for most of the cases. We also find that the distribution of the values of the  $\beta$  coefficient both in increasing and narrow magnitude intervals shows a maximum at  $M_B \sim -18 \pm 1$ . We perform non-parametric tests on the  $\beta$  coefficient data

and they indicate that the variations are real and that there is evidence of an underlying trend, that is, there is evidence that the  $\beta$  coefficient changes systematically when we consider brighter galaxies and that the value of this coefficient attains a maximum value at  $M_B \sim -18 \pm 1$  and smaller values at the extremes of the magnitude spectrum available.

- We perform numerical simulations of the different samples of galaxies under study. The results of the analysis of the variation of the KR coefficients, both in increasing and in narrow magnitude intervals show that the coefficients depend on the width and brightness of the magnitude range and that this dependence comes as a result of a geometrical effect due to the fact that:
  - The distribution of galaxies on the  $\log(r_e) - <\mu>_e$  plane depends on luminosity, and
  - That the geometric shape of the distribution of the galaxies on this plane is not symmetrical (see Sect. 4 for full details).
- Finally, numerical simulations confirm the fact that the intrinsic dispersion of the KR depends on the magnitude range, as asserted in Nigoche-Netro *et al.* (2007).

From the previously mentioned results, it is very important to establish that if the magnitude range is not taken into consideration when performing comparisons of galaxy samples such as the dependence of the KR on the environment, on redshift or on wavelength, the differences which might be found may be misinterpreted.

## Acknowledgments

We would like to thank Project WINGS (Fasano *et al.* 2002, Varela 2004) for providing the photometric parameters for the samples in 7 Abell clusters, Consejo Nacional de Ciencia y Tecnología (México) for a PhD fellowship number 132526, Ministerio Español de Educación y Ciencia for grant PNAYA2006, Instituto de Matemáticas y Física Fundamental (CSIC, España) and Instituto de Astronomía (UNAM, México) for all the facilities provided for the realization of this project. We would also like to record our obligation to Mariano Moles for help with the presentation of this paper.

## References

- Aguerri, J. L. A., Iglesias-Páramo, J., Vílchez, J. M., Muñoz-Tuñón, C., & Sánchez-Janssen, R. 2005, *ApJ*, 130, 475
- Akritis, M. G., & Bershad, M. A. 1996, *ApJ*, 470, 706
- Bendat J. S., & Piersol A. G. 1966. *Measurement and Analysis of Random Data*. Ed. Wiley J. & Sons. New York.
- Bender, R., Burstein, D., & Faber S. M. 1996, *ApJ*, 463, L51
- Bernardi, M., *et al.* 2003, *AJ*, 125, 1817
- Bernardi, M., *et al.* 2003b, *AJ*, 125, 1849
- Bernardi, M., *et al.* 2007, *AJ*, 133, 1741
- Bernardi, M., *et al.* 2007b, *AJ*, 133, 1954
- Capaccioli, M., Caon, N., & D’Onofrio, M. 1992, *MNRAS*, 259, 323
- Colberg, J. M., *et al.* 2000, *MNRAS*, 319, 209
- Djorgovsky, S., & Davies, M. 1987, *ApJ*, 313, 59
- D’Onofrio, M., Valentinuzzi, T., Secco, L., Caimmi, R., & Bindoni, D. 2006, *NewAR*, 50, 447
- Dressler, A., Lynden-Bell, D., Burstein, D., Davies, R. L., Faber, S. M., Terlevich, R., & Wegner, G. 1987, *ApJ*, 313, 42
- Fasano, G., Bettoni, D., Marmo, C., Pignatelli, E., Poggianti, B. M., Moles, M., & Kjærgaard, P. 2002, *ASPC*, 268, 361
- Fasano, G., Varela, J., Bettoni, D., *et al.* 2004, Private communication.
- Fukugita, M., Ichikawa, T., Gunn, J. E., Doi, M., Shimasaku, K., & Schneider D. P. 1996, *AJ*, 111, 4

- Graham, A. W., & Driver, S. P. 2005. PASP, 22, 118
- Graham, A., & Guzmán, R. 2003, AJ, 125, 2936
- Hamabe, M., & Kormendy, J. 1987, In: Structure and Dynamics of Elliptical Galaxies, IAU Symp., No 127, p.379, ed. de Zeeuw, T., Reidel, Dordrecht
- Hoessel, J. G., Oegerle, W. R., & Schneider, D. P. 1987, AJ, 94, 1111
- Isobe, T., Feigelson, E. D., Akritas, M. G., & Babu, G. J. 1990, ApJ, 364, 104
- Jorgensen, I., Franx, M., & Kærgaard, p. 1996, MNRAS, 280, 167
- Jorgensen, I., Franx, M., Hjorth, J., & van Dokkum, P. G. 1999, MNRAS, 308, 833
- Kelson, D.D., van Dokkum, P. G., Franx, M., Illingworth, G. D., & Fabricant, D. 1997, ApJ, 478, L13
- Kjærgaard, P., Jorgensen, I., & Moles, M. 1993, ApJ, 418, 617
- Kormendy, J., 1977, ApJ, 218, 333
- La Barbera, F., Busarello, G., & Capaccioli, M. 2000, A&A, 362, 851
- La Barbera, F., Busarello, G., Merluzzi, P., Massarotti, M., & Capaccioli M. 2003, ApJ, 595, 127
- Michard, R., 2000, A&A, 360, 85
- Milvang-Jensen, B. 1997, Master's Thesis. University of Copenhagen
- Nigoche-Netro, A., Moles, M., Ruelas-Mayorga, A., Franco-Balderas, A., & Kjærgaard, P. 2007, A&A, 472, 773
- Nigoche-Netro, A. 2007, PhD Thesis. Universidad Complutense de Madrid
- Prugniel, P., & Siemen, F. 1997, A&A, 321, 111
- Reda, F. M., Forbes, D. A., Beasley, M., O'Sullivan, E. J., & Goudfrooij, P. 2004, MNRAS, 354, 851
- Sandage, A., & Peremulter, J-M. 1991, ApJ, 370, 455
- Sandage, A., & Lubin, L. M. 2001, ApJ, 121, 2271
- Varela, J. 2004, PhD Thesis. Universidad Complutense de Madrid

## **Appendix A: Tables with behavior of the KR coefficients with respect to absolute magnitude range.**

**Table A.1.** KR coefficients for the different galaxy samples in increasing intervals of magnitude. MI is the total absolute magnitude interval within which the galaxies are distributed, N is the number of galaxies in the magnitude interval,  $\alpha_{Bis}$  is the zero point of KR,  $\beta_{Bis}$  is the slope of KR,  $\sigma_{KR}$  is the intrinsic dispersion of KR and R is the correlation coefficient of the fit (Pearson Statistics).

MI	N	$\alpha_{Bis}$	$\beta_{Bis}$	$\sigma_{KR}$	R	MI	N	$\alpha_{Bis}$	$\beta_{Bis}$	$\sigma_{KR}$	R
Abell (V)						Coma (Gunn r)					
$-16 \geq M > -17$	136	21.997±0.063	4.733±0.268	0.201	0.933	$-17 \geq M > -18$	17	20.019±0.138	2.537±0.276	0.536	0.802
$-16 \geq M > -18$	284	21.232±0.075	5.949±0.274	0.488	0.834	$-17 \geq M > -19$	68	19.377±0.111	3.266±0.313	0.692	0.705
$-16 \geq M > -19$	394	20.917±0.116	5.721±0.411	0.719	0.715	$-17 \geq M > -20$	82	19.302±0.095	3.281±0.229	0.667	0.769
$-16 \geq M > -20$	519	20.574±0.190	5.216±0.630	1.031	0.504	$-17 \geq M > -21$	109	19.135±0.093	3.210±0.219	0.656	0.743
$-16 \geq M > -21$	593	20.967±0.216	3.102±0.673	1.143	0.326	$-17 \geq M > -22$	169	18.917±0.090	2.982±0.167	0.674	0.725
$-16 \geq M > -22$	626	21.229±0.155	2.070±0.445	1.143	0.251	$-17 \geq M > -23$	192	18.824±0.092	2.687±0.173	0.711	0.645
$-16 \geq M > -23$	...	...	...	...	...	$-17 \geq M > -24$	196	18.837±0.089	2.598±0.158	0.708	0.651
Hydra (Gunn r)											
$-18 \geq M > -19$	4	19.722±0.024	5.037±0.062	0.077	0.996						
$-18 \geq M > -20$	15	18.964±0.122	5.721±0.158	0.378	0.961						
$-18 \geq M > -21$	42	18.295±0.151	5.277±0.213	0.685	0.885						
$-18 \geq M > -22$	54	18.068±0.170	5.097±0.256	0.824	0.813						
SDSS (g*)						SDSS (r*)					
$-18.5 \geq M > -19$	26	18.392±0.040	4.808±0.100	0.128	0.982	$-18.5 \geq M > -19$	3	...	...	...	...
$-18.5 \geq M > -20$	517	18.978±0.027	4.726±0.057	0.297	0.900	$-18.5 \geq M > -20$	77	18.962±0.051	4.645±0.138	0.258	0.929
$-18.5 \geq M > -21$	2856	18.686±0.020	3.909±0.033	0.362	0.825	$-18.5 \geq M > -21$	1014	18.204±0.025	4.356±0.050	0.322	0.877
$-18.5 \geq M > -22$	6687	18.790±0.016	3.057±0.021	0.406	0.763	$-18.5 \geq M > -22$	4057	17.963±0.019	3.609±0.030	0.386	0.784
$-18.5 \geq M > -23$	8516	18.949±0.014	2.641±0.016	0.425	0.744	$-18.5 \geq M > -23$	7646	18.093±0.015	2.858±0.020	0.418	0.724
$-18.5 \geq M > -24$	8661	18.989±0.013	2.572±0.015	0.425	0.749	$-18.5 \geq M > -24$	8630	18.214±0.013	2.572±0.017	0.426	0.717
$-18.5 \geq M > -25$	...	...	...	...	...	$-18.5 \geq M > -24.7$	8666	18.225±0.013	2.552±0.016	0.426	0.721
SDSS (i*)						SDSS (z*)					
$-19 \geq M > -20$	31	17.458±0.059	4.717±0.209	0.219	0.937	$-19.5 \geq M > -20$	15	17.331±0.038	4.482±0.104	0.116	0.984
$-19 \geq M > -21$	505	18.033±0.027	4.540±0.062	0.311	0.894	$-19.5 \geq M > -21$	210	17.940±0.035	4.742±0.085	0.299	0.908
$-19 \geq M > -22$	2805	17.605±0.020	3.941±0.036	0.371	0.816	$-19.5 \geq M > -22$	1799	17.312±0.022	4.259±0.042	0.358	0.850
$-19 \geq M > -23$	6645	17.663±0.015	3.047±0.022	0.406	0.741	$-19.5 \geq M > -23$	5440	17.264±0.017	3.309±0.025	0.400	0.765
$-19 \geq M > -24$	8512	17.808±0.013	2.598±0.013	0.422	0.716	$-19.5 \geq M > -24$	8277	17.437±0.013	2.680±0.017	0.414	0.738
$-19 \geq M > -25$	8664	17.843±0.012	2.529±0.016	0.422	0.723	$-19.5 \geq M > -25$	8658	17.504±0.012	2.543±0.015	0.413	0.748
$-19 \geq M > -26$	...	...	...	...	...	$-19.5 \geq M > -25.3$	8665	17.507±0.012	2.537±0.015	0.413	0.750

**Table A.2.** KR coefficients for the different galaxy samples in narrow 1 *mag* intervals. MI is the total absolute magnitude interval within which the galaxies are distributed, N is the number of galaxies in the magnitude interval,  $\alpha_{Bis}$  is the zero point of KR,  $\beta_{Bis}$  is the slope of KR,  $\sigma_{KR}$  is the intrinsic dispersion of KR and R is the correlation coefficient of the fit (Pearson Statistics).

MI	N	$\alpha_{Bis}$	$\beta_{Bis}$	$\sigma_{KR}$	R	MI	N	$\alpha_{Bis}$	$\beta_{Bis}$	$\sigma_{KR}$	R
Abell (V)						Coma (Gunn r)					
-16.0 $\geq M >$ -17.0	136	21.997 $\pm$ 0.063	4.733 $\pm$ 0.268	0.201	0.933	-17.0 $\geq M >$ -18.0	17	20.019 $\pm$ 0.138	2.537 $\pm$ 0.276	0.536	0.802
-17.0 $\geq M >$ -18.0	148	21.009 $\pm$ 0.051	5.276 $\pm$ 0.193	0.275	0.924	-18.0 $\geq M >$ -19.0	51	19.087 $\pm$ 0.111	3.783 $\pm$ 0.256	0.623	0.772
-18.0 $\geq M >$ -19.0	110	20.223 $\pm$ 0.082	4.886 $\pm$ 0.319	0.310	0.918	-19.0 $\geq M >$ -20.0	14	18.957 $\pm$ 0.081	3.243 $\pm$ 0.090	0.316	0.970
-19.0 $\geq M >$ -20.0	125	19.128 $\pm$ 0.044	4.983 $\pm$ 0.093	0.287	0.929	-20.0 $\geq M >$ -21.0	27	18.015 $\pm$ 0.044	4.839 $\pm$ 0.077	0.182	0.971
-20.0 $\geq M >$ -21.0	74	18.310 $\pm$ 0.070	4.791 $\pm$ 0.120	0.289	0.926	-21.0 $\geq M >$ -22.0	51	17.427 $\pm$ 0.052	4.685 $\pm$ 0.067	0.251	0.965
-21.0 $\geq M >$ -22.0	33	18.246 $\pm$ 0.071	3.830 $\pm$ 0.072	0.146	0.941	-22.0 $\geq M >$ -23.0	32	16.879 $\pm$ 0.035	4.512 $\pm$ 0.156	0.221	0.936
-22.0 $\geq M >$ -23.0	...	...	...	...	...	-23.0 $\geq M >$ -24.0	4	17.087 $\pm$ 0.057	3.569 $\pm$ 0.211	0.243	0.894
Hydra (Gunn r)											
-18.0 $\geq M >$ -19.0	4	19.722 $\pm$ 0.024	5.037 $\pm$ 0.062	0.077	0.996						
-19.0 $\geq M >$ -20.0	11	18.994 $\pm$ 0.115	5.255 $\pm$ 0.167	0.312	0.968						
-20.0 $\geq M >$ -21.0	27	17.902 $\pm$ 0.063	5.127 $\pm$ 0.078	0.237	0.987						
-21.0 $\geq M >$ -22.0	12	17.142 $\pm$ 0.112	4.821 $\pm$ 0.148	0.240	0.974						
SDSS (g*)						SDSS (r*)					
-18.5 $\geq M >$ -19.0	26	18.392 $\pm$ 0.040	4.808 $\pm$ 0.100	0.128	0.982	-18.5 $\geq M >$ -19.0	3	...	...	...	...
-19.0 $\geq M >$ -20.0	491	18.922 $\pm$ 0.021	4.760 $\pm$ 0.044	0.238	0.936	-19.0 $\geq M >$ -20.0	74	18.864 $\pm$ 0.035	4.966 $\pm$ 0.091	0.220	0.948
-20.0 $\geq M >$ -21.0	2339	18.254 $\pm$ 0.013	4.463 $\pm$ 0.021	0.249	0.918	-20.0 $\geq M >$ -21.0	937	18.036 $\pm$ 0.014	4.619 $\pm$ 0.028	0.233	0.937
-21.0 $\geq M >$ -22.0	3831	17.590 $\pm$ 0.014	4.277 $\pm$ 0.017	0.245	0.912	-21.0 $\geq M >$ -22.0	3043	17.366 $\pm$ 0.011	4.342 $\pm$ 0.018	0.244	0.914
-22.0 $\geq M >$ -23.0	1829	16.874 $\pm$ 0.023	4.279 $\pm$ 0.023	0.223	0.927	-22.0 $\geq M >$ -23.0	3589	16.624 $\pm$ 0.014	4.320 $\pm$ 0.017	0.242	0.905
-23.0 $\geq M >$ -24.0	145	16.386 $\pm$ 0.086	4.118 $\pm$ 0.072	0.161	0.951	-23.0 $\geq M >$ -24.0	984	16.016 $\pm$ 0.027	4.224 $\pm$ 0.028	0.199	0.934
-24.0 $\geq M >$ -25.0	...	...	...	...	...	-24.0 $\geq M >$ -24.7	36	15.474 $\pm$ 0.162	4.162 $\pm$ 0.132	0.151	0.953
SDSS (i*)						SDSS (z*)					
-19.0 $\geq M >$ -20.0	31	17.458 $\pm$ 0.059	4.717 $\pm$ 0.209	0.219	0.937	-19.5 $\geq M >$ -20.0	15	17.331 $\pm$ 0.038	4.482 $\pm$ 0.104	0.116	0.984
-20.0 $\geq M >$ -21.0	474	17.926 $\pm$ 0.018	4.713 $\pm$ 0.039	0.235	0.941	-20.0 $\geq M >$ -21.0	195	17.859 $\pm$ 0.024	4.838 $\pm$ 0.056	0.229	0.986
-21.0 $\geq M >$ -22.0	2300	17.213 $\pm$ 0.012	4.481 $\pm$ 0.021	0.249	0.918	-21.0 $\geq M >$ -22.0	1589	17.065 $\pm$ 0.013	4.610 $\pm$ 0.024	0.246	0.980
-22.0 $\geq M >$ -23.0	3840	16.572 $\pm$ 0.012	4.250 $\pm$ 0.016	0.241	0.904	-22.0 $\geq M >$ -23.0	3641	16.475 $\pm$ 0.011	4.213 $\pm$ 0.015	0.236	0.980
-23.0 $\geq M >$ -24.0	1867	15.877 $\pm$ 0.020	4.239 $\pm$ 0.023	0.219	0.918	-23.0 $\geq M >$ -24.0	2837	15.831 $\pm$ 0.015	4.142 $\pm$ 0.018	0.223	0.977
-24.0 $\geq M >$ -25.0	152	15.212 $\pm$ 0.068	4.240 $\pm$ 0.062	0.160	0.956	-24.0 $\geq M >$ -25.0	381	15.308 $\pm$ 0.035	4.027 $\pm$ 0.033	0.158	0.973



**Table A.3.** KR coefficients for the SDSS simulation in  $r^*$  filter. Increasing magnitude intervals. MI is the total absolute magnitude interval within which the galaxies are distributed, N is the number of galaxies in the magnitude interval,  $\alpha_{Bis}$  is the zero point of KR,  $\beta_{Bis}$  is the slope of KR,  $\sigma_{KR}$  is the intrinsic dispersion of KR and R is the correlation coefficient of the fit (Pearson Statistics).

MI	N	$\alpha_{Bis}$	$\beta_{Bis}$	$\sigma_{KR}$	R	MI	N	$\alpha_{Bis}$	$\beta_{Bis}$	$\sigma_{KR}$	R
Case 1						Case 2					
$-20 \geq M > -21$	455	18.587 $\pm$ 0.015	4.971 $\pm$ 0.011	0.285	0.995	$-20 \geq M > -21$	140	18.533 $\pm$ 0.020	4.356 $\pm$ 0.032	0.234	0.968
$-20 \geq M > -22$	810	18.232 $\pm$ 0.022	4.865 $\pm$ 0.017	0.555	0.977	$-20 \geq M > -22$	280	18.313 $\pm$ 0.020	3.604 $\pm$ 0.023	0.330	0.953
$-20 \geq M > -23$	1065	18.029 $\pm$ 0.025	4.673 $\pm$ 0.022	0.785	0.945	$-20 \geq M > -23$	420	18.270 $\pm$ 0.019	3.213 $\pm$ 0.018	0.365	0.961
$-20 \geq M > -24$	1220	17.977 $\pm$ 0.025	4.442 $\pm$ 0.027	0.953	0.907	$-20 \geq M > -24$	560	18.277 $\pm$ 0.018	3.014 $\pm$ 0.013	0.381	0.971
$-20 \geq M > -25$	1275	17.995 $\pm$ 0.025	4.305 $\pm$ 0.031	1.030	0.885	$-20 \geq M > -25$	676	18.311 $\pm$ 0.017	2.872 $\pm$ 0.011	0.388	0.976
Case 3											
$-20 \geq M > -21$	245	18.602 $\pm$ 0.018	4.819 $\pm$ 0.025	0.275	0.984						
$-20 \geq M > -22$	439	18.360 $\pm$ 0.022	4.305 $\pm$ 0.027	0.478	0.943						
$-20 \geq M > -23$	579	18.338 $\pm$ 0.023	3.708 $\pm$ 0.028	0.585	0.906						
$-20 \geq M > -24$	664	18.412 $\pm$ 0.026	3.268 $\pm$ 0.029	0.627	0.889						
$-20 \geq M > -25$	669	18.474 $\pm$ 0.027	3.053 $\pm$ 0.028	0.640	0.887						

**Table A.4.** KR coefficients for the SDSS simulation for  $r^*$  filter. Narrow 1 mag intervals. MI is the total absolute magnitude interval within which the galaxies are distributed, N is the number of galaxies in the magnitude interval,  $\alpha_{Bis}$  is the zero point of KR,  $\beta_{Bis}$  is the slope of KR,  $\sigma_{KR}$  is the intrinsic dispersion of KR and R is the correlation coefficient of the fit (Pearson Statistics).

MI	N	$\alpha_{Bis}$	$\beta_{Bis}$	$\sigma_{KR}$	R	MI	N	$\alpha_{Bis}$	$\beta_{Bis}$	$\sigma_{KR}$	R
Case 1						Case 2					
$-20 \geq M > -21$	455	18.587 $\pm$ 0.015	4.971 $\pm$ 0.011	0.285	0.995	$-20 \geq M > -21$	140	18.533 $\pm$ 0.020	4.356 $\pm$ 0.032	0.234	0.968
$-21 \geq M > -22$	355	17.614 $\pm$ 0.020	4.953 $\pm$ 0.016	0.284	0.992	$-21 \geq M > -22$	140	17.810 $\pm$ 0.024	4.356 $\pm$ 0.032	0.234	0.968
$-22 \geq M > -23$	255	16.677 $\pm$ 0.031	4.912 $\pm$ 0.025	0.280	0.985	$-22 \geq M > -23$	140	17.087 $\pm$ 0.033	4.356 $\pm$ 0.032	0.234	0.968
$-23 \geq M > -24$	155	15.878 $\pm$ 0.060	4.786 $\pm$ 0.048	0.270	0.963	$-23 \geq M > -24$	140	16.364 $\pm$ 0.045	4.356 $\pm$ 0.032	0.234	0.968
$-24 \geq M > -25$	55	15.727 $\pm$ 0.200	4.305 $\pm$ 0.147	0.212	0.885	$-24 \geq M > -25$	140	15.788 $\pm$ 0.069	4.356 $\pm$ 0.032	0.234	0.968
Case 3											
$-20 \geq M > -21$	245	18.602 $\pm$ 0.018	4.819 $\pm$ 0.025	0.275	0.984						
$-21 \geq M > -22$	194	17.709 $\pm$ 0.024	4.735 $\pm$ 0.032	0.269	0.976						
$-22 \geq M > -23$	140	16.984 $\pm$ 0.037	4.508 $\pm$ 0.043	0.253	0.960						
$-23 \geq M > -24$	85	16.697 $\pm$ 0.068	4.028 $\pm$ 0.065	0.218	0.925						
$-24 \geq M > -25$	35	17.391 $\pm$ 0.168	3.097 $\pm$ 0.119	0.140	0.891						

